Applied Composite Materials (2026) 33:81
https://doi.org/10.1007/s10443-026-10463-4

RESEARCH

A High-Fidelity Numerical Study of Trans-Laminar Fracture in Carbon/Epoxy Laminates Under Varying Environmental Conditions

Xiaodong Xu[1] **· Supratik Mukhopadhyay**[2]

Received: 22 November 2025 / Accepted: 9 March 2026 / Published online: 27 March 2026
© The Author(s) 2026

Abstract
This paper focuses on trans-laminar fracture process under varying environmental conditions which is crucial for the design and certification of many modern engineering applications. High-fidelity Finite Element (FE) models are developed for predicting trans-laminar fracture of a quasi-isotropic carbon/epoxy laminate under room temperature dry, and for the first time hot temperature wet conditions. Such FE modelling of ASTM E1922 specimens has not been done before. The FE models in ABAQUS Explicit employ a Weibull failure criterion for fibre fracture and cohesive surfaces for sub-critical damage to explain the complex trans-laminar fracture process. It successfully captures the toughening mechanisms, which are further enhanced by increased sub-critical damage under hot temperature wet conditions. This can finally be confirmed by the current models which addresses some limitations of ASTM E1922 e.g. a limited ligament length and the tendency of having premature compressive failure at the specimen rear end.

Keywords Fracture toughness · Fracture · Finite Element Analysis (FEA) · Environmental conditions

1 Introduction

The failure behaviour of composites is very complex. A major issue is trans-laminar fracture propagation due to stress concentrations at notches in composite structures. The importance of this issue has been recognised and studied by the National Aeronautics and Space Administration (NASA) [1], Airbus [2] and the Japan Aerospace Exploration Agency (JAXA) [3]. However, currently it is difficult to predict this, and extensive testing is required.

✉ Xiaodong Xu
xiaodong.xu@cranfield.ac.uk

[1] Centre for Aeronautics, Faculty of Engineering and Applied Sciences, College Road, Cranfield MK43 0AL, UK

[2] Department of Mechanical Engineering, Indian Institute of Technology, Kanpur 208016, India

There is an ASTM E1922 standard for trans-laminar fracture toughness for polymer matrix composites [4]. It has been adopted to characterise trans-laminar fracture toughness of different materials [5–7], fracture process zone development [8] and hygrothermal effects [9]. Its limitations have been pointed out through experimental studies, such as small ligament size and undesirable compressive failure at the specimen rear end. To the authors' best knowledge, no numerical studies based on the ASTM E1922 standard have been conducted to understand trans-laminar fracture behaviour.

Predicting fracture behaviour is challenging due to the interaction of complex failure mechanisms. Different methods have been developed for example, continuum damage mechanics [10–14], finite fracture mechanics [15], smeared crack method [16], cohesive zone method [17], machine learning [18], phase field method [19] and peridynamics method [20]. Another modelling method is discrete crack method [21–23] which can model failure mechanisms explicitly such as fibre fracture, matrix cracking and delamination and their interaction. Li et al. [21] adopted cohesive elements and a stress-based Weibull failure criterion. It is different from an energy-based fibre failure criterion by Ruta et al. [23] that required additional trans-laminar fracture energy inputs. Compared to Ruta et al. [23], a complex process is needed for generating cohesive elements for all interfaces and a network of potential splitting paths following the method developed by Li et al. [24]. Methods for trans-laminar fracture response at elevated temperatures and wet conditions are however very limited, such as this analytical study [25].

Trans-laminar fracture of quasi-isotropic carbon/epoxy laminates has been successfully predicted at both room temperature dry and hot temperature wet conditions, which has not been done before. It is also the first known Finite Element (FE) modelling of the ASTM E1922 standard tests which is the only designated ASTM standard for measuring trans-laminar fracture toughness of polymer-based composites. The current high-fidelity FE method uses the advanced general contact option in ABAQUS Explicit, so the complex meshing process for cohesive elements is no longer needed. Addressing the limitations of the experiments as per the ASTM E1922 standard, the FE model helps explain the trans-laminar fracture behaviour at varying environmental conditions.

2 Modelled Experiments

The modelled geometry is Eccentrically loaded Single Edge-notched Tension (ESET) specimen according to the ASTM E1922 standard as shown in Fig. 1 [4]. The specimens were cut using a Computer Numerical Controlled (CNC) router using 1 mm diameter end mills. The machined edge notch was then sharpened manually using 0.25 mm thick precise saw blades. The material used is Hexcel's HexPly® IM7/8552 unidirectional prepreg, and the stacking sequence is $[90/45/0/-45]_{4s}$.

The experiments were conducted as per the ASTM E1922 standard [4] at Room Temperature Dry (RTD) [8] and Hot Temperature Wet (HTW) [9] conditions. The HTW specimens were conditioned at 80 °C and 85% relative humidity until full saturation and then tested in an environmental chamber at 120 °C and dry conditions. The HTW specimens refer to hot-wet conditioned specimens tested hot-dry thereafter. The static test duration was short so the loss of moisture during hot-dry tests was ignored [9].

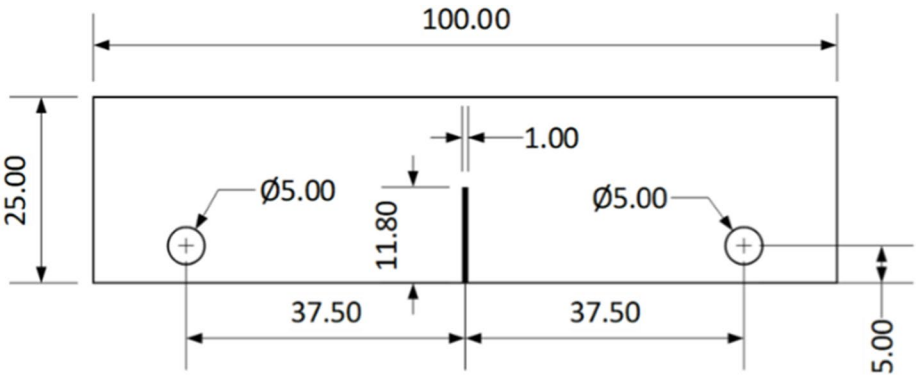

Fig. 1 ESET specimen geometry before notch sharpening [4]

An effective crack length was defined to include a Fracture Process Zone (FPZ) where the 0° plies are broken but some ± 45° plies are still intact [22]. The combined true crack length where all plies are broken plus the length of broken 0° plies within FPZ constitutes the effective crack length.

The stress intensity factor, *K*, is calculated by Eq. (1) in the ASTM E1922 standard [4]:

$$K = \frac{\frac{P}{B\sqrt{W}}\alpha^{\frac{1}{2}}\left(1.4+\alpha\right)\left[3.97-10.88\alpha+26.25\alpha^{2}-38.9\alpha^{3}+30.15\alpha^{4}-9.27\alpha^{5}\right]}{\left(1-\alpha\right)^{\frac{3}{2}}} \quad (1)$$

where P is the failure load at the load drops, a represents the effective crack length considering the modelled fibre breakage in the 0° plies, B is the specimen thickness, W is the specimen width and $\alpha = a/W$.

The strain energy release rate, *G*, is calculated by the following Eq. (2) assuming plane stress:

$$G = \frac{K^2}{E} \quad (2)$$

where E = 61.6 GPa is the Young's modulus of the laminate.

3 Finite Element (FE) Method

The FE method was implemented in ABAQUS Explicit with C3D8R continuum elements. The baseline mesh is generated from a unit cell based on Li et al. [24]. Recently, the same meshing method in ABAQUS was used to predict tension-tension fatigue failure but trans-laminar fracture was not covered [26]. A ply-by-ply half model is created from the unit cells within a region of 24 mm × 12 mm × 2 mm ahead of the pre-defined crack. The rest of the regions were modelled using the same C3D8R continuum element blocks but with homogenised properties in Table 1. The mesh details are shown in Fig. 2. The minimum mesh size is 0.25 mm in the unit-cell region, and the maximum mesh size is 3.25 mm further away.

Table 1 Homogenised properties for IM7/8552 [31]

E_1=E_2(GPa)	E_3(GPa)	G_{13}=G_{23}(GPa)	G_{12}(GPa)	ν_{13}= ν_{23}	ν_{12}
61.6	13.5	4.5	23.4	0.31	0.32

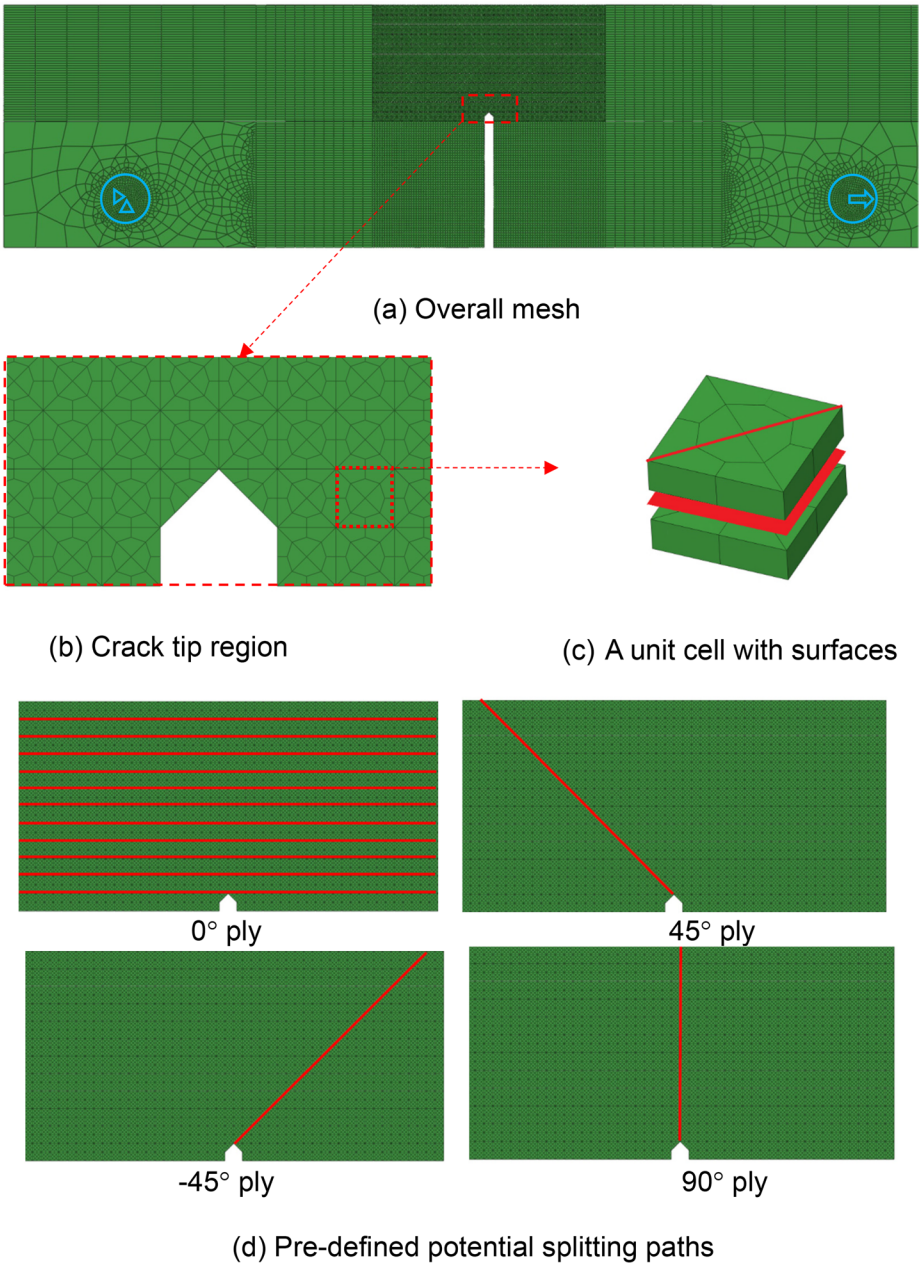

Fig. 2 FE mesh details with unit cells

Table 2 Cohesive interface properties for IM7/8552 [27]

t_n^{RTD} (MPa)	t_s^{RTD} (MPa)	G_{IC}^{RTD} (kJ/m^2)	G_{IIC}^{RTD} (kJ/m^2)	t_n^{HTW} (MPa)	t_s^{HTW} (MPa)	G_{IC}^{HTW} (kJ/m^2)	G_{IIC}^{HTW} (kJ/m^2)	e
60	90	0.26	1.0	44.5	48.2	0.35	0.41	1

Table 3 Ply properties for IM7/8552 [31]

E_1(GPa)	E_2=E_3(GPa)	G_{12}=G_{13}(GPa)	G_{23}(GPa)	ν_{12}= ν_{13}	ν_{23}	σ_{unit}(MPa)	m
161	11.4	5.17	3.98	0.32	0.44	3131	41

Symmetry boundary conditions were used through the model thickness. Along the loading direction, displacements were fixed at one loading pin, while a prescribed velocity was applied at the opposite loading pin end at a constant rate of 2 mm/s. Semi-automatic mass scaling was used with a target timestep of 1×10^{-6} s. Despite a higher loading rate than that in the experiments and the use of mass scaling, the kinetic energy is within 6.2% of internal energy during fracture propagation, to ensure a quasi-static loading condition.

Following the previous study using LS-Dyna [22], the ABAQUS model was divided into two different mesh regions: a ply-by-ply unit-cell mesh region and a blocked structural mesh region to reduce computational costs. Unlike the previous study using a complex meshing algorithm for cohesive elements [18], cohesive surfaces were pre-defined between the plies within the unit-cell region (Fig. 2c) using the ABAQUS general contact. Within the unit-cell region, potential splitting paths are created within each ply as shown in Fig. 2d. The interfaces between the unit-cell mesh region and the remaining element block were connected using tie constrains. The same cohesive surface approach and properties were used for splitting as for other interfaces. The mix-mode behaviour was represented by a power law with an exponent of $e = 1$. The properties for the cohesive surfaces listed in Table 2 are from the literature [27]. The elastic properties are assumed not to depend on the environmental conditions.

Finally, a fibre failure criterion [21] was adopted according to Weibull theory [28]. Weibull theory was adopted to predict fibre failure in continuous fibre composites [22, 26, 27] and discontinuous composites [29, 30]. In this work, it uses the fibre-direction stress in all plies within the unit-cell region to predict failure according to Eq. (3). When Eq. (3) is satisfied, $\sigma_{u,i}$, is the critical fibre-direction stress in the i_{th} ply. The element with the maximum fibre-direction stress will be deleted to simulate fibre failure.

$$\sum_{i=1}^{\text{Number of elements}} V_i \left(\sigma_{u,i}/\sigma_{\text{unit}}\right)^m = 1 \tag{3}$$

where $\sigma_{u,i}$ is the fibre-direction tensile stress in the i_{th} element, V_i is the volume of the i_{th} element, σ_{unit} is the tensile strength of a unit volume of material, and m is the Weibull modulus from the previous work. All material properties used are listed in Tables 3 and 1.

The focus of this paper is to predict progressive trans-laminar fracture in ABAQUS. Compressive failure at the specimen rear end was not modelled so some experimental limitations can be addressed.

4 FE Modelling Results

4.1 FE Model Verification at Room Temperature Dry Conditions

The FE models were run using 64 cores on a high-performance computer cluster at Cranfield University. The FE results are compared to the previous experimental results at RTD conditions [8] as shown in Fig. 3a. The FE model captures the overall load vs. Pin Opening Displacement (POD) response well, including the peak loads and key load drops. However, the FE model is stiffer than the specimens, which could be caused by the compliance in the test jig. For easier comparison of the loads, the FE displacements were scaled to match the experimental stiffness. Only loads were used for fracture analyses.

The predicted load-displacement response is also verified against the typical test of Specimen 1 at approximately circled loads in Fig. 3b. The predicted damage states are compared with the in situ X-ray Computed Tomography (CT) scans images of Specimen 1 [8] in Fig. 4. A good agreement has been reached between the modelled and observed damage states. Please note that delamination is not visible in the CT scan images, but fibre fracture and splitting are comparable with the FE results.

All plies through the thickness are predicted broken after the peak load as shown in Fig. 5 indicated by the removed elements in 0°, 45° and −45° plies. This is consistent with the experimental observation [8]. In the experiment the last load drop was triggered by compressive failure at the specimen rear end which is not modelled.

4.2 FE Results at Hot Temperature Wet Conditions

Since the FE model correlates well with the experiments at RTD conditions, it is also used to explain the trans-laminar fracture response at HTW conditions [9]. The FE model captures the overall response as seen in Fig. 6.

It was observed that specimens at HTW conditions have more damage than that at RTD conditions. This has been seen in the current HTW model and compared reasonably to the CT scan image of a 0° ply in Fig. 7. Such extensive damage can delay fibre failure, resulting in a 75% increase of trans-laminar fracture energy [9].

5 Discussion

A good agreement up to peak load has been reached between the current models and experiments until the onset of compressive failure, with the predicted post-peak crack growth interpreted as an idealized extension rather than a reproduction of the physical tests.

At RTD conditions, the model can continue to run after reaching the peak value without pre-mature compressive failure observed in the ESET tests. The load envelope appears to follow a Linear Elastic Fracture Mechanics (LEFM) line as shown in Fig. 8. The LEFM line is determined by Eq. 1 and constant fracture energy of 100 kJ/m^2 which is derived from the peak load and corresponding effective crack length. This implies that the fracture process zone has been fully developed using the current model geometry following the ASTM

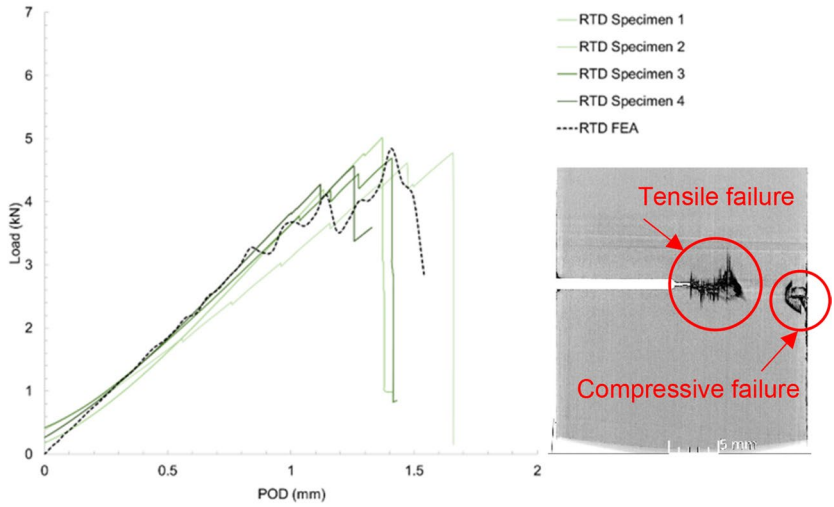

(a) Comparison with a CT image of a failed specimen.

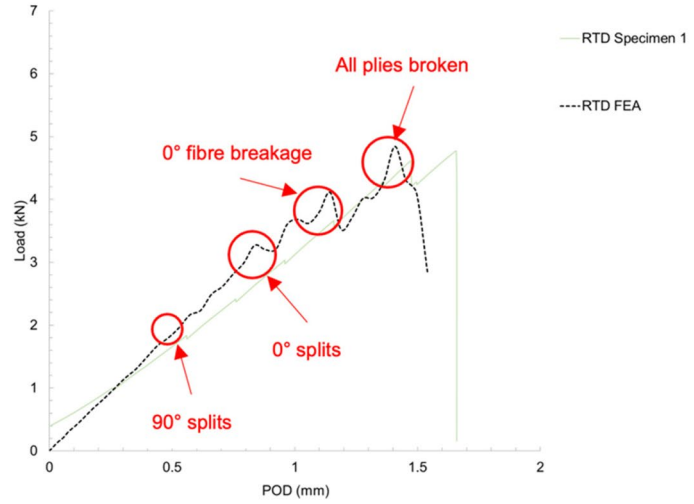

(b) Comparison against *in situ* test

Fig. 3 Comparison between experimental and FE results at room temperature dry conditions. (**a**) Comparison with a CT image of a failed specimen, (**b**) Comparison against in situ test

E1922 standard [4]. However, this analysis can only be done numerically, because compressive failure stopped any further crack growth around the peak load in the experiments due to the limitation of a small specimen [9].

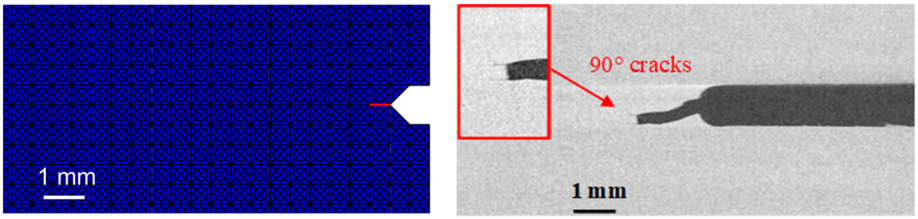

(a) 90° splitting early on (in red marked manually)

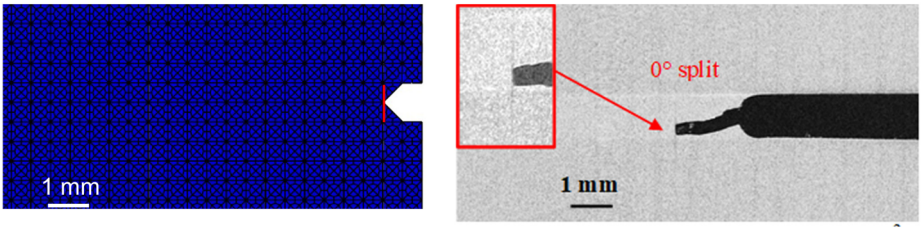

(b) 0° damage without fibre breakage (in red marked manually)

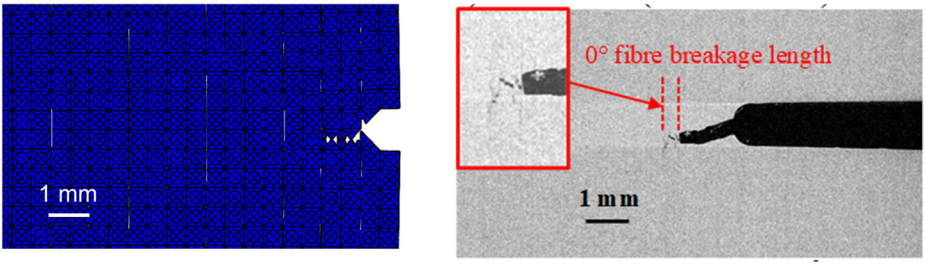

(c) First 0° fibre breakage (represented by removed elements)

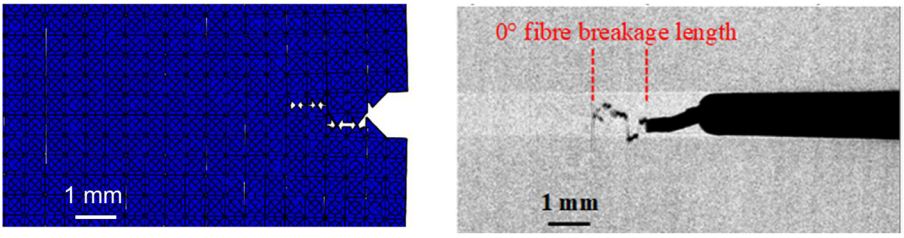

(d) Further 0° fibre breakage (represented by removed elements)

Fig. 4 Predicted damage compared with in situ CT scans [8] at similar loads at room temperature dry conditions

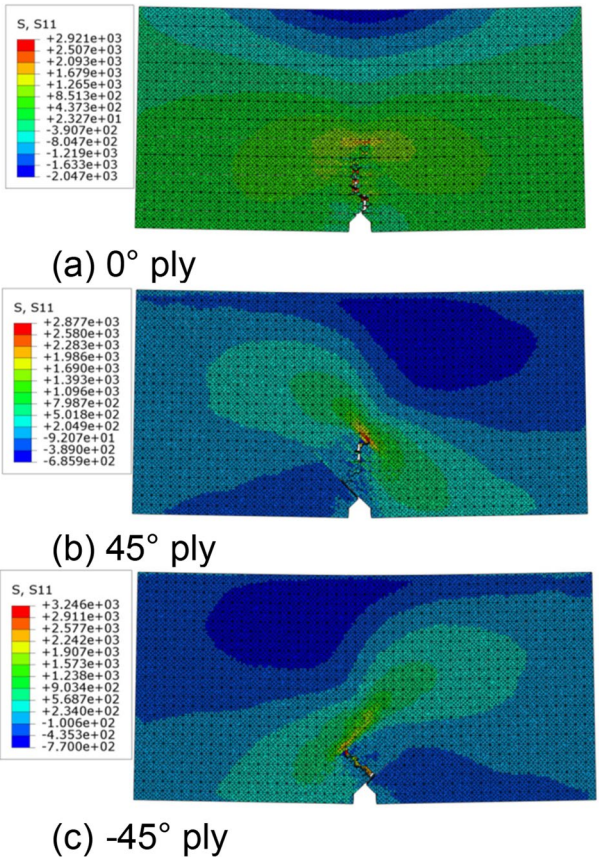

Fig. 5 Fibre direction stress distributions just after the peak load of 4.84 kN (100 kJ/m^2) at room temperature dry conditions

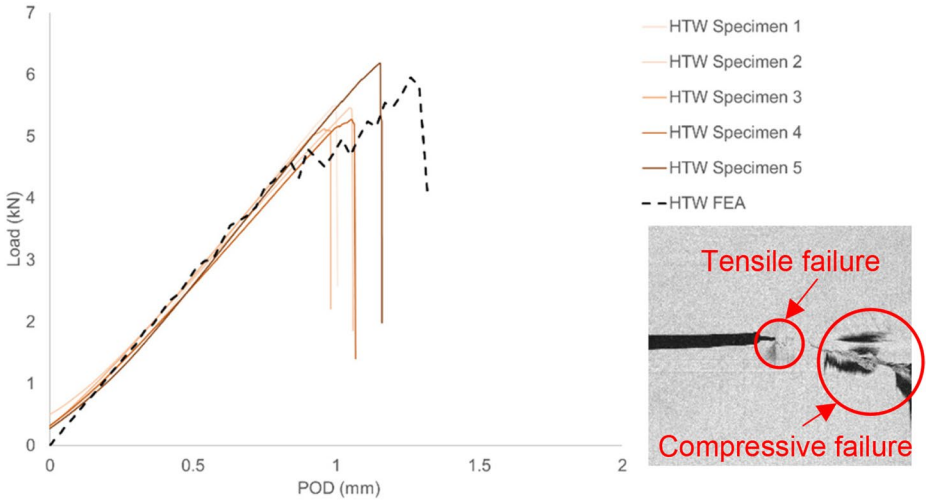

Fig. 6 Comparison between experimental and FE results at hot temperature wet conditions

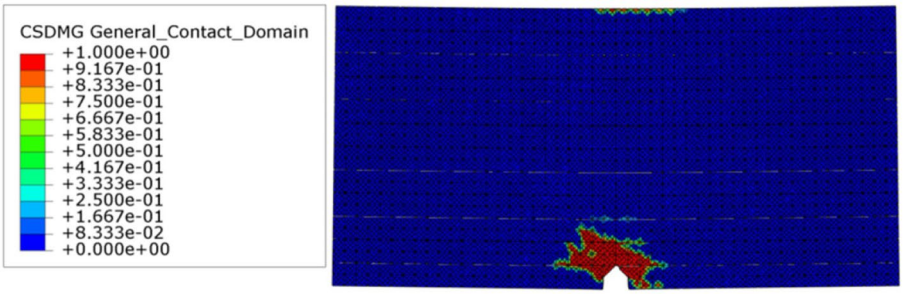

(a) Damage before fibre breakage

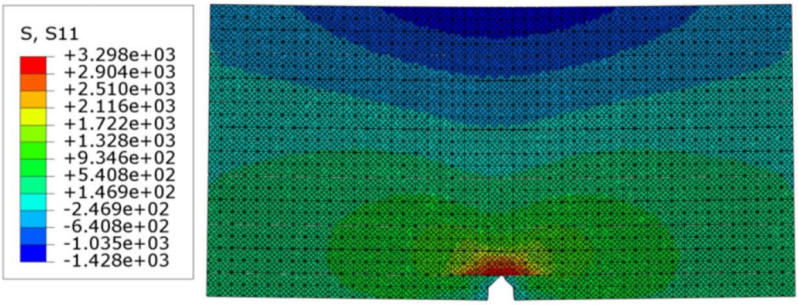

(b) Fibre direction stress distribution

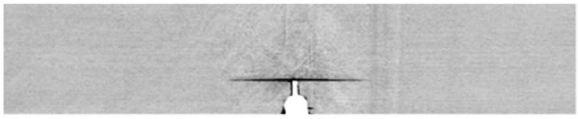

(c) 0° ply splitting in a CT scan image [9]

Fig. 7 Damage and stress distribution in a typical 0° ply before fibre failure at hot temperature wet conditions

At HTW conditions, the model captures the peak load well without considering compressive failure at the specimen rear end. This implies that the measured peak load was likely to be triggered by the significant propagation of the crack under tension immediately followed by compressive failure at the rear end. Had premature compressive failure occurred in the experiments, the model would have overpredicted. The model implies that most plies are already broken through the thickness at the peak load. The extensive matrix damage in the 45° plies also suggests a large damage height contributing to much higher G_{max} value of 217.1 kJ/m^2 at HTW conditions than RTD (100 kJ/m^2). However, this numerical observation cannot be fully verified experimentally again due to the limitations of the experiments which limited sufficient crack propagation [9].

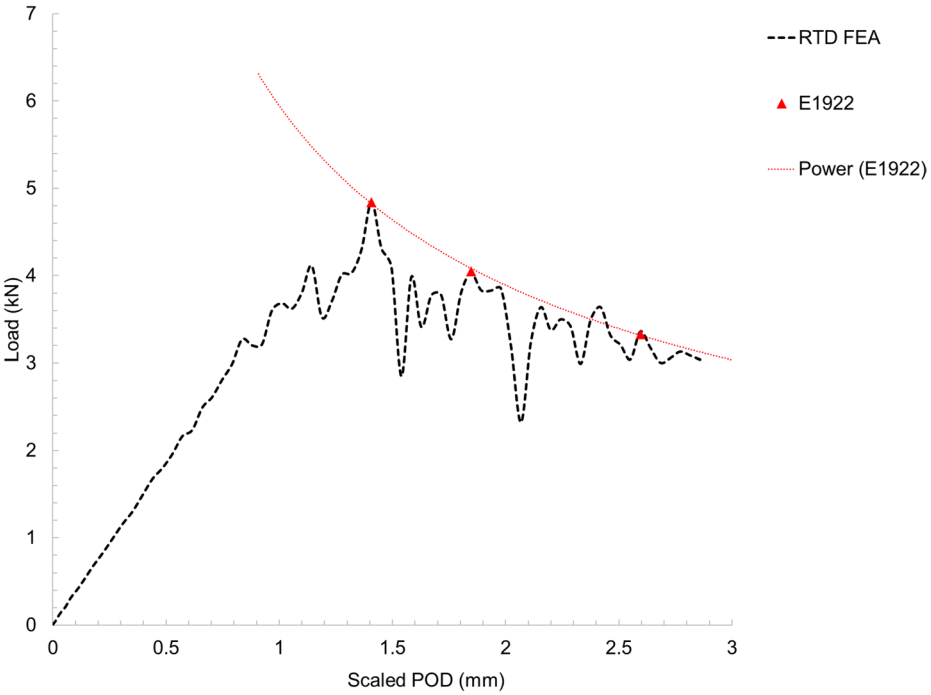

Fig. 8 Predicted post-peak fracture behaviour at room temperature dry conditions

6 Conclusions

This paper successfully addresses the engineering challenge of accurately modelling notched failures in advanced composites at varying environmental conditions.

The current FE model in ABAQUS Explicit confirms that a much tougher trans-laminar fracture response at HTW conditions is due to the degradation of some key matrix properties, which leads to extensive sub-critical damage and delays fibre breakage from the notch tip.

The FE model explained the trans-laminar fracture sequence by excluding the compressive failure mode at the model rear end, which was found to be impossible to avoid experimentally, due to the limitations of specimen size and the building-up of undesirable compressive stress at the specimen rear end.

Acknowledgements In memory of Dr. Xianqian Li, whose guidance and invaluable contributions profoundly benefited the authors.

Authors' contributions Xiaodong Xu: Conceptualization, Investigation, Methodology, Writing - original draft. Supratik Mukhopadhyay: Investigation, Software, Writing - Reviewing & Editing.

Funding No funding was received for conducting this study.

Data Availability All data supporting the findings of this study are available within the paper.

Declarations

Competing interests The authors declare no competing interests.

Open Access This article is licensed under a Creative Commons Attribution 4.0 International License, which permits use, sharing, adaptation, distribution and reproduction in any medium or format, as long as you give appropriate credit to the original author(s) and the source, provide a link to the Creative Commons licence, and indicate if changes were made. The images or other third party material in this article are included in the article's Creative Commons licence, unless indicated otherwise in a credit line to the material. If material is not included in the article's Creative Commons licence and your intended use is not permitted by statutory regulation or exceeds the permitted use, you will need to obtain permission directly from the copyright holder. To view a copy of this licence, visit http://creativecommons.org/licenses/by/4.0/.

References

1. Bergan, A., Bakuckas, J., Awerbuch, J., Tan, T.M.: Assessment of damage containment features of a full-scale PRSEUS fuselage panel. Compos. Struct. **113**, 174–185 (2014). https://doi.org/10.1016/j.compstruct.2014.03.011
2. Fualdes, C.: The Composite Airframe: How to Keep Attractiveness? In: 23rd International Conference on Composite Materials., Belfast (2023)
3. Aoki, Y., Takeda, S., Shoji, H., Sugimoto, S., Iwahori, Y.: Evaluation on discrete source damages of CFRP stiffened panels. In: 28th International Congress of the Aeronautical Sciences,., Brisbane (2012)
4. ASTM E1922-04: : Standard Test Method for Translaminar Fracture Toughness of Laminated and Pultruded Polymer Matrix Composite Materials., West Conshohocken (2015) (2015)
5. Sun, X., Takeda, S., Wisnom, M.R., Xu, X.: In situ characterization of trans-laminar fracture toughness using X-ray Computed Tomography. Compos. Commun. **21**, 100408 (2020). https://doi.org/10.1016/j.coco.2020.100408
6. Saadati, Y., Lebrun, G., Bouvet, C., Chatelain, J.-F., Beauchamp, Y.: Study of translaminar fracture toughness of unidirectional flax/epoxy composite. Compos. Part. C: Open. Access. **1**, 100008 (2020). https://doi.org/10.1016/j.jcomc.2020.100008
7. Kumar, V., Veer, P., Rayasam, S., Makireddypalli Adinarayanappa, S.: Experimental Investigation of Fracture Behavior of 3D Printed Nano-alumina Reinforced Polylactic Acid Composites Using Compact-Tension Tests and Infrared Thermography. J. Mater. Eng. Perform. (2023). https://doi.org/10.1007/s11665-023-09066-y
8. Xu, X., Takeda, S., Wisnom, M.R.: Investigation of fracture process zone development in quasi-isotropic carbon/epoxy laminates using in situ and ex situ X-ray Computed Tomography. Compos. Part. Appl. Sci. Manuf. **166**, 107395 (2023). https://doi.org/10.1016/j.compositesa.2022.107395
9. Gong, B., Ge, Y., Wang, H., Peng, H.-X., Wisnom, M.R., Xu, X.: Hygrothermal effects on translaminar fracture toughness of quasi-isotropic laminates with different stacking sequences. Compos. Commun. **45**, 101791 (2024). https://doi.org/10.1016/j.coco.2023.101791
10. Dávila, C.G., Camanho, P.P., Rose, C.A.: Failure criteria for FRP laminates. J. Compos. Mater. **39**, 323–345 (2005). https://doi.org/10.1177/0021998305046452
11. Pinho, S.T., Iannucci, L., Robinson, P.: Physically based failure models and criteria for laminated fibre-reinforced composites with emphasis on fibre kinking. Part II: FE implementation. Compos. Part. Appl. Sci. Manuf. **37**, 766–777 (2006). https://doi.org/10.1016/j.compositesa.2005.06.008
12. Li, X., Qu, P., Kong, H., Zhu, Y., Hua, C., Guo, A., Wang, S.: Multi-scale numerical analysis of damage modes in 3D stitched composites. Int. J. Mech. Sci. **266**, 108983 (2024). https://doi.org/10.1016/j.ijmecsci.2024.108983
13. Kirar, E., Kisa, M., Ozen, M., Demircan, G., Guven, C.: Mechanical properties of glass/epoxy composites under artificial seawater environment: Numerical simulation and experimental validation. Mar. Struct. **98**, 103679 (2024). https://doi.org/10.1016/j.marstruc.2024.103679
14. Kirar, E., Demircan, G.: Aging-Sensitive Damage Modelling of FRPs: Calibration and Validation. Appl. Compos. Mater. **33**, 39 (2025). https://doi.org/10.1007/s10443-025-10424-3
15. Camanho, P.P., Erçin, G.H., Catalanotti, G., Mahdi, S., Linde, P.: A finite fracture mechanics model for the prediction of the open-hole strength of composite laminates. Compos. Part. Appl. Sci. Manuf. **43**, 1219–1225 (2012). https://doi.org/10.1016/j.compositesa.2012.03.004

16. Forghani, A., Zobeiry, N., Vaziri, R., Poursartip, A., Ellyin, F.: A non-local approach to simulation of damage in laminated composites. 26th Annual Technical Conference of the American Society for Composites 2011 and the 2nd Joint US-Canada Conference on Composites. 1, (2011)
17. Ortega, A., Maimí, P., González, E.V., Trias, D.: Characterization of the translaminar fracture Cohesive Law. Compos. Part A Appl. Sci. Manuf. **91**, 501–509 (2016). https://doi.org/10.1016/j.compositesa.2016.01.019
18. Zobeiry, N., Reiner, J., Vaziri, R.: Theory-guided machine learning for damage characterization of composites. Compos. Struct. **246**, 112407 (2020). https://doi.org/10.1016/j.compstruct.2020.112407
19. Tan, W., Martínez-Pañeda, E.: Phase field fracture predictions of microscopic bridging behaviour of composite materials. Compos. Struct. **286**, 115242 (2022). https://doi.org/https://doi.org/ https://doi.org/10.1016/j.compstruct.2022.115242
20. Qu, P., Kong, H., Li, X., Lei, Y., Guo, A., Wang, S., Wang, H., Hu, Y., Wan, Y., Takahashi, J.: Additive manufacturing of hybrid continuous carbon/basalt fiber reinforced composites based on bi-matrix co-extrusion. J. Mater. Res. Technol. **30**, 8683–8704 (2024). https://doi.org/10.1016/j.jmrt.2024.05.241
21. Li, X., Hallett, S.R., Wisnom, M.R.: A finite element based statistical model for progressive tensile fibre failure in composite laminates. Compos. B Eng. **45**, 433–439 (2013). https://doi.org/10.1016/j.compositesb.2012.08.001
22. Xu, X., Wisnom, M.R., Hallett, S.R.: Deducing the R-curve for trans-laminar fracture from a virtual Over-height Compact Tension (OCT) test. Compos. Part A Appl. Sci. Manuf. **118**, 162–170 (2019). https://doi.org/10.1016/j.compositesa.2018.12.027
23. Rutar, R., Bouvet, Christophe, Serra, J.: Numerical simulation and R-curves computation of CFRP compact tension tests using the discrete ply model. J. Compos. Mater. **59**, 2025–2047 (2025). https://doi.org/10.1177/00219983251324064
24. Li, X., Hallett, S.R., Wisnom, M.R.: Modelling the effect of gaps and overlaps in automated fibre placement (AFP)-manufactured laminates. Sci. Eng. Compos. Mater. **22**, 115–129 (2015). https://doi.org/10.1515/secm-2013-0322
25. Yu, B., Katafiasz, T.J., Nguyen, S., Allegri, G., Finlayson, J., Greenhalgh, E.S., Pinho, S.T., Pimenta, S.: Hygrothermal effects on the translaminar fracture toughness of a highly toughened aerospace CFRP: Experimental characterisation and model prediction. Compos. Part. Appl. Sci. Manuf. **150**, 106582 (2021). https://doi.org/10.1016/j.compositesa.2021.106582
26. Zhang, B., Ali, H., Allegri, G., Hallett, S.R.: An experimental and numerical investigation into tensile fatigue failure of composite laminates containing wrinkles and cut plies. Int. J. Fatigue. **198**, 109026 (2025). https://doi.org/10.1016/j.ijfatigue.2025.109026
27. Sengodan, G.A., Allegri, G., Hallett, S.R.: Simulation of progressive failure in laminated composites under variable environmental conditions. Mater. Des. **196**, 109082 (2020). https://doi.org/10.1016/j.matdes.2020.109082
28. Weibull, W.: A statistical distribution function of wide applicability, (1951). http://web.cecs.pdx.edu/~cgshirl/Documents/Weibull-ASME-Paper-1951.pdf
29. Jesus, A., Xu, X.: Rapid prediction of fibre-dominant tensile failure in randomly oriented strands. J. Reinf. Plast. Compos. **42**, 205–212 (2023). https://doi.org/10.1177/07316844221107927
30. Xu, X., Jesus, A., Wan, Y., Takahashi, J.: A stochastic modelling framework for predicting flexural properties of ultra-thin randomly oriented strands. Adv. Compos. Mater 1–15. https://doi.org/10.1080/09243046.2024.2351667
31. Xu, X., Millen, S.L.J., Mitchard, D., Wisnom, M.R.: On residual tensile strength after lightning strikes. Compos. Part. Appl. Sci. Manuf. **194**, 108899 (2025). https://doi.org/10.1016/j.compositesa.2025.108899

Publisher's Note Springer Nature remains neutral with regard to jurisdictional claims in published maps and institutional affiliations.

DSPACE

https://dspace.org/

A high-fidelity numerical study of trans-laminar fracture in carbon/epoxy laminates under varying environmental conditions

Xu, Xiaodong; Mukhopadhyay, Supratik

2026-04
Springer
https://doi.org/10.1007/s10443-026-10463-4
Xu X, Mukhopadhyay S. (2026) A high-fidelity numerical study of trans-laminar fracture in carbon/epoxy laminates under varying environmental conditions. Applied Composite Materials, Volume 33, Issue 2, April 2026, Article number 81

Downloaded from a DSpace repository. https://dspace.org/